

A climatology of the stratopause in WACCM and the zonally asymmetric elevated stratopause

J. A. France^{1,2} and V. L. Harvey^{1,2}

Received 6 September 2012; revised 16 January 2013; accepted 22 January 2013; published 15 March 2013.

[1] A climatology of the stratopause is produced using a 40 year simulation of the Whole Atmosphere Community Climate Model (WACCM). Anomalies in polar winter stratopause temperature and height are interpreted with respect to the location of the polar vortices and anticyclones. The WACCM climatology is compared to an 8 year climatology based on Microwave Limb Sounder (MLS) observations and data from the Goddard Earth Observing System (GEOS) version 5 from August 2004 to July 2012. The WACCM climatology is in excellent agreement with observations, except in the Antarctic vortex where the WACCM stratopause is \sim 10K warmer and \sim 5 km higher than observations. WACCM diabatic heating rates support the hypothesis that ageostrophic vertical motions associated with baroclinic planetary waves are responsible for producing Arctic winter temperature anomalies. The area of the winter polar vortices in WACCM at the stratopause is 30% smaller in the NH and 45% smaller in the SH compared to GEOS. The long WACCM record allows us to explore the geographical distribution and temporal evolution of a composite of 15 elevated stratopause (ES) events. This composite is in good agreement with the 2012 ES event observed by MLS, though December ES events in WACCM are not observed by MLS. This is the first work to show that ES events are not zonally symmetric. In the 30 days following ES events, the ES composite shows that the stratopause altitude is highest over the Canadian Arctic, and the highest stratopause temperatures occur 90° to the east over the Norwegian Sea.

Citation: France, J. A., and V. L. Harvey (2013), A climatology of the stratopause in WACCM and the zonally asymmetric elevated stratopause, *J. Geophys. Res. Atmos.*, 118, 2241–2254, doi:10.1002/jgrd.50218.

1. Introduction

[2] The stratopause is characterized by a warm layer at \sim 50 km that is produced by the absorption of ultraviolet radiation by ozone at sunlit latitudes. In the polar night, the stratopause is maintained by gravity wave (GW)-driven diabatic descent [e.g., Hitchman *et al.*, 1989]. France *et al.* [2012] (hereafter referred to as [F12]) used 7 years of temperature data from the Microwave Limb Sounder (MLS) to define the stratopause and the Goddard Earth Observing System Model (GEOS) version 5 analyses to denote the polar vortices and anticyclones. F12 showed that the stratopause temperature and height depends on the location of the polar winter vortices and anticyclones.

[3] In general, planetary waves (PWs) propagate vertically only where there are weak westerly winds

[Charney and Drazin, 1961]. The geographic structure of stratopause temperature and height in the Arctic winter is dominated by frequent weather events that are driven by vertically propagating baroclinic PWs [e.g., Thayer *et al.*, 2010]. These waves affect the stratopause temperature because they result in nonlinear wave interactions, turbulence, as well as breaking PWs that lead to Eliassen-Palm (EP) flux divergence and subsequent ageostrophic circulations [e.g., Andrews *et al.*, 1987]. Because of this dynamical control on stratopause temperature, it is of interest to determine the extent to which the Whole Atmosphere Community Climate Model (WACCM) reproduces the observed stratopause structure. Here we reproduce the analysis in F12 using a multi-decadal WACCM simulation and compare the model climatology to 8 years of MLS observations.

[4] Previous work demonstrates the ability of Global Climate Models (GCMs) to reproduce the climatological polar winter stratopause during undisturbed periods [e.g., Braesicke and Langematz, 2000; Volodin and Schmitz, 2001; Becker, 2012]. Because the winter stratopause is dynamically driven, properly simulating the stratopause in a GCM is dependent on the parameterization of gravity waves (GWs) [Becker, 2012; McLandress *et al.*, 2012]. Volodin and Schmitz [2001] used the Institute for Numerical Mathematics (INM) Atmospheric General Circulation Model (AGCM)

¹Laboratory for Atmospheric and Space Physics, University of Colorado, Boulder, Colorado, USA.

²Department of Atmospheric and Oceanic Sciences, University of Colorado, Boulder, Colorado, USA.

Corresponding author: J. A. France, University of Colorado, 3665 Discovery Drive, Boulder, CO 80303, USA. (jeffrey.france@colorado.edu)

©2013. American Geophysical Union. All Rights Reserved.
2169-897X/13/10.1002/jgrd.50218

with a Doppler-spread non-orographic parameterization for GWs to show that the Arctic (Antarctic) polar stratopause height in January (July) is 5–10K (\sim 10K) warmer than the Committee on Space Research (COSPAR) 1986 International Reference Atmosphere (CIRA-86) [Fleming et al., 1990]. Becker [2012] used the Kühlingsborn Mechanistic general Circulation Model (KMCM), which explicitly determines GWs, to show that Arctic stratopause temperatures in January are up to 20K warmer than the CIRA-86 climatology. In both of these studies, the dynamically driven polar winter stratopause is shown to be strongly dependent on the GW parameterization scheme used in the model. See McLandress and Scinocca [2005] for a comparison of the fidelity of different GW parameterizations in global models.

[5] Recent model studies of the Arctic winter have focused on the ability of the model to reproduce stratospheric sudden warmings (SSWs) and elevated stratopause (ES) events [e.g., Charlton et al., 2007; Siskind et al., 2007, 2010; de la Torre et al., 2012]. SSWs are characterized by rapid warming in the polar stratosphere and a weakening of the polar night jet. ES events observed in 2004, 2006, 2009, and 2012 are characterized by a rapid reformation of the Arctic polar winter stratopause near 80 km [e.g., Manney et al., 2005; 2008; 2009]. Charlton et al. [2007] evaluated six different models (including WACCM version 1) to determine how well they simulated SSWs. They found that the models were capable of reproducing SSWs, but the frequency at which they produced them was generally too low. De la Torre et al. [2012] produced a climatology of SSWs and ES events using WACCM version 3.5.48. The four WACCM runs used in their study are free running, use the radiative conditions between 1953 and 2006, and have slightly different initial conditions. Based on these runs, they found that WACCM produced SSWs at a rate of 0.45 to 0.7 events per year, comparing well to the 0.6 events per year observed in the National Centers for Environmental Prediction and the National Center for Atmospheric Research (NCEP/NCAR) and the European Centre for Medium-Range Weather Forecasts (ECMWF) re-analysis (ERA) between 1957/58 and 2001/02 [Charlton and Polvani, 2007].

[6] Most ES events occur in conjunction with prolonged major SSWs. De la Torre et al. [2012] showed that WACCM effectively reproduces the zonal mean evolution of ES events compared with observations [e.g., Manney et al., 2008; 2009]. ES events have been well documented in WACCM [Kvissel et al., 2011; Marsh 2011; Chandran et al., 2011; Limpasuvan et al., 2011], and WACCM version 4 has been shown to be capable of producing ES events that closely resemble observed frequencies [Chandran et al., 2013]. Chandran et al. [2013] show a zonal mean composite evolution of ES events in WACCM and their relationship to SSWs. Their results show that on average, 2–4 ES events occur each decade, which is about half the frequency of SSWs [de la Torre et al., 2012]. The multi-decadal nature of the model record is of value here to expand on their results and document the zonally asymmetric geographic structure of an ES composite.

[7] Given the coherent structure of the polar vortex, a physically intuitive approach to analyze stratospheric

variability is to use information of vortex geometry. Geometric moments reflect the movement of the vortex about the pole, vortex area, vortex elongation, and vortex splitting [Melander et al., 1986; Waugh, 1997; Waugh and Randel, 1999; Dritschel, 1993; Matthewman et al., 2009; Mitchell et al., 2011; Hannachi et al., 2011]. Mitchell et al. [2011] compared SSW composites based on vortex moment diagnostics to a SSW composite based on traditional zonal mean definitions. Their results indicate that the traditional SSW definition often fails to identify extreme disruptions to the vortex. They also caution against categorizing SSW events as “vortex displacement” versus “vortex split” and suggest that most SSW events demonstrate characteristics of both types as they evolve in time and space. We further the work of Mitchell et al. [2011], which relies on a PV-based definition of the vortex [Nash et al., 1996], by using a more robust definition of the vortex that can be applied in the upper stratosphere and mesosphere [Harvey et al., 2002; Harvey et al., 2009]. The structure of the vortex in the upper stratosphere and mesosphere can be used to evaluate any GCM, as is done in this analysis with WACCM.

[8] An outline of this paper is as follows. Section 2 describes WACCM, MLS, GEOS, and the analysis methods used. Section 3 presents the 40 year stratopause climatology in WACCM and compares it to an 8 year climatology based on MLS observations. Results include the mean annual cycle of zonal mean stratopause temperature and height as a function of latitude; a representative case study that demonstrates the dynamical mechanism responsible for the climatological zonally asymmetric stratopause structures observed in the Arctic; 40 year monthly mean polar maps of stratopause temperature, height, and vertical motion in both hemispheres; seasonal averages showing the vertical structure of temperature, the polar vortices, and anticyclones as a function of longitude; and the temporal evolution of stratopause temperature and height inside the polar vortex and anticyclone regions. Section 5 is devoted to highlighting the 15 ES events identified in the 40 year simulation. The timing, spatial structure, and longitude-altitude structure of ES events in WACCM are compared to MLS. Conclusions are given in section 6.

2. Global Model, Satellite Data, and Analysis Methods

2.1. WACCM

[9] The Whole Atmosphere Community Climate Model version 4.0.3 (WACCM) is a fully coupled general circulation model that extends from the Earth's surface to \sim 145 km [Garcia et al., 2007, and references therein]. WACCM is based on the Community Atmosphere Model version 4 (CAM4), which has a finite-volume dynamical core [Lin, 2004]. The chemistry in WACCM is from the Model for Ozone and Related Chemical Tracers version 3 (MOZART3) [Kinnison et al., 2007]. WACCM includes parameterizations for both orographic GWs based on McFarlane [1987] and non-orographic GWs [Richter et al., 2010]. In WACCM versions 3.5 and 4, the arbitrarily specified parameterization for non-orographic GWs has been replaced by two distinct parameterizations, including one for deep convection [Beres et al., 2005] and a second for frontal systems [Richter

et al., 2010]. The horizontal resolution of the model is 1.9° latitude by 2.5° longitude. There are 66 vertical levels with a vertical resolution increasing from 1.1 km in the lower stratosphere to 1.75 km near the stratopause and to ~ 3.5 km above ~ 65 km [Garcia *et al.*, 2007].

2.2. MLS

[10] The MLS instrument, onboard NASA's Aura satellite, is in a 705 km Sun-synchronous orbit [Waters *et al.*, 2006]. MLS samples ~ 3500 profiles each day that are spaced 165 km along the satellite track that span 82°S to 82°N . MLS temperature is inferred from 118 GHz oxygen emission. This work uses version 3 temperature data [Livesey *et al.*, 2011]. The temperature measurements have a vertical resolution of ~ 5.5 km at ~ 3 hPa and ~ 8 km at 0.01 hPa. Temperature precision is $\sim 1\text{K}$ in the upper stratosphere, and there is a $\sim 1\text{K}$ cold bias in MLS temperature based on coincident comparisons [Schwartz *et al.*, 2008; Livesey *et al.*, 2011]. MLS temperatures have uncertainties ranging from 0.6K in the stratosphere to 2.5K in the mesosphere and are filtered using version 3 status, quality, threshold, and convergence values from the MLS science team [Livesey *et al.*, 2011].

2.3. Goddard Earth Observing System (GEOS)

[11] The GEOS model version 5 uses an Atmospheric General Circulation Model (AGCM) and the Gridpoint Statistical Interpolation to generate the Data Assimilation System. The dynamics that are integrated into the GEOS AGCM are from the Earth System Modeling Framework [Rienecker *et al.*, 2007]. For this analysis, GEOS version 5.1 is used prior to 1 September 2008 after which we use GEOS version 5.2.

[12] Pressure, temperature, geopotential height, and horizontal winds are provided every 6 h at 72 equally spaced vertical levels from 1 km to 72 km on a 0.5° latitude by 0.67° longitude grid. In this work, daily averaged products are linearly interpolated to a 2.5° latitude by 3.75° longitude grid and to potential temperature levels ranging from 300K (~ 10 km) to 4000K (~ 70 km). The potential temperature levels chosen correspond to a vertical resolution of ~ 2 km in the upper stratosphere and lower mesosphere. The algorithm used to demark the polar vortices and anticyclones is an extension of the method described by Harvey *et al.* [2002], which accounts for circumpolar anticyclones. We interpolate this "vortex marker" field to the height of the stratopause.

2.4. Analysis Methods

[13] The polar vortices and anticyclones are defined in WACCM using the method described by Harvey *et al.* [2002], with an improvement that properly identifies circumpolar anticyclones. This method determines the location of the vortices and anticyclones by calculating closed integrals of Q , which is a scalar quantity that is a measure of the relative strain versus rotation in the wind field [e.g., Harvey *et al.*, 2002]. We interpolate this "vortex marker" field to the height of the stratopause. The stratopause is defined using the method described by F12. Briefly, the stratopause is determined for individual temperature profiles by the following method: (1) apply an 11 km boxcar smoothing in the vertical coordinate to each

temperature profile, (2) determine the maximum temperature between 20 and 80 km (T_{\max_smooth}), (3) find local temperature maxima in the unsmoothed temperature profile within 15 km of T_{\max_smooth} , and (4) require the lapse rate to be positive for 5 km below and negative for 5 km above the maximum temperature. If one level meets these criteria, then it is defined as the stratopause. Using this method, $\sim 4\%$ of temperature profiles have no stratopause defined. This generally occurs in the polar night when the GW-driven descent is disrupted and there is no mechanism to maintain the warm stratopause, or in the case of ageostrophic ascent and cooling associated with vertically propagating PW energy.

[14] The following method is used to identify ES events. We first determine an area-weighted mean vertical temperature profile poleward of 70°N for each day. The data are fit to a 200 m vertical grid between 15 and 100 km using a sixth-order polynomial similar to the method used by McDonald *et al.* [2011] and Day *et al.* [2011]. We define the stratopause to be the maximum temperature between 20 km and 100 km. At the onset of an ES event, the polar atmosphere often becomes isothermal between ~ 30 km and ~ 80 km, and the stratopause becomes ill-defined. As a result, small temperature variations can cause large fluctuations in the height of the stratopause from day to day. In order to accommodate the spurious variability in stratopause height during these times, the average stratopause height is computed for days 3–7 prior to each day ($Z-$) and 3–7 days following each day ($Z+$). For an ES candidate to be considered, we require that the difference between $Z+$ and $Z-$ exceed 10 km. We choose 10 km because it separates two distinct populations of vertical jumps in stratopause height, and here we are interested only in the events with the greater vertical displacement in stratopause height. Once a candidate ES is identified, we define ES event onset as the first day in which the daily mean stratopause height increases by at least 25 km compared to the previous day. We choose 25 km because it delineates a distinct population of ES events where both the stratopause reformed at high altitudes and the atmosphere was isothermal at the time of reformation. This threshold results in ES frequencies that are consistent with previous work. To compute the duration of ES events, we consider the stratopause to be elevated until it descends in altitude below one standard deviation above the 40 year daily mean. This method is valid because the polar cap average stratopause height descends smoothly with time following ES events. In our analysis of ES events, we compare a composite of 15 ES events identified in WACCM to the ES event observed by MLS in 2012. While the ES events observed by MLS in 2006 and 2009 do not show the same structure as the event in 2012, we show the 2012 event to demonstrate that a zonally asymmetric elevated stratopause has been observed. The ES events are removed from the climatology shown in section 3 and are considered separately in section 4.

3. WACCM Stratopause Climatology

3.1. Latitude-Time Evolution of the Climatological Stratopause

[15] Figure 1 shows the 40 year WACCM (left) and 8 year MLS (right) zonally averaged annual cycle of

stratopause temperature (top panels) and height (bottom panels) as a function of latitude. We apply a 7 day running mean at each latitude to reduce day-to-day variability. Thick black and white contours encompass regions where the vortex and anticyclones are present for at least 50% of the time, respectively.

[16] WACCM effectively reproduces the large-scale stratopause features and seasonal evolution shown by MLS and previous work [Barnett, 1974; Labitzke, 1974; Hood, 1986; Hitchman and Leovy, 1986; F12]. In particular, WACCM simulates the “separated” stratopause in the winter polar vortices. The tropical semiannual oscillation is also reproduced by WACCM. This oscillation occurs as a result of seasonal variations in solar zenith angle and the amount of insolation. The anticyclones in the SH move from mid-latitudes in winter to high latitudes in spring as the vortex weakens. The SH stratopause remains elevated in August and slowly descends from 58 km to 46 km from August to November. To this point, the longest climatology of the stratopause is the 7 year climatology from F12; thus, this is the first time the structure and seasonal variations at the stratopause are shown to be robust over multiple decades. Major differences between WACCM and MLS observations include the following:

- In the NH, the polar-separated stratopause in WACCM is \sim 10–15K warmer than MLS from October to March.

- In the NH, the stratopause in the vortex is 3–8 km higher than that in MLS in January, February, and March.
- In the Antarctic vortex, WACCM stratopause temperatures are up to 30K warmer than that in MLS.
- In the Antarctic vortex, the separated stratopause in WACCM is \sim 10 km higher than that in MLS and remains elevated 2 months longer.
- The Antarctic vortex in WACCM persists 1 month longer at the stratopause than it does in GEOS. This is consistent with the results of Sun [2010], who showed that the date of the final warming in WACCM occurs on average 20 days later than in NCEP/NCAR. The reason for this delay is likely due to too little orographic GW drag [e.g., McLandress *et al.*, 2012].

3.2. Case Study

[17] In the NH, F12 showed that the daily distribution of stratopause temperature and height displays a large degree of zonal asymmetry associated with westward tilting baroclinic PWs (see their Figure 2). For brevity, Figure 2 shows a single day to illustrate that WACCM reproduces these weather events. Polar plots of (a) stratopause temperature and (b) stratopause height on 10 December are shown during an arbitrary model year. Longitude-altitude sections at 60° N of (c) eddy temperature (zonal mean is removed) and (d) eddy potential temperature tendency ($d\theta/dt$) highlight wave-1 zonal asymmetries. The edges of the polar

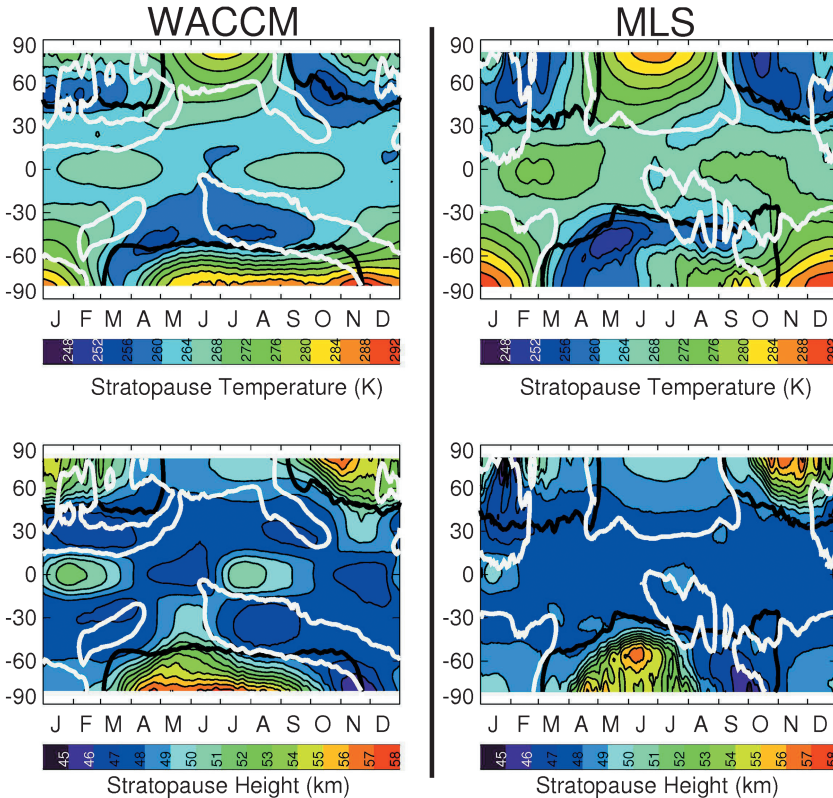


Figure 1. Latitude-time plot of the average annual cycle of stratopause temperature (top) and height (bottom) based on WACCM (left) and MLS (right). The annual cycle in WACCM (MLS) is based on 40 (8) years of model output (satellite data). Thick black and white contours encompass regions where the vortex and anticyclones occur at least 5% of the time, respectively. For WACCM, the vortex and anticyclones are based on WACCM winds. For MLS, the vortex and anticyclones are based on GEOS winds.

vortex and anticyclones are denoted by the thick black and white contours, respectively, and in the longitude-altitude sections, the thick gray contour denotes the stratopause. $d\theta/dt$ is representative of diabatic vertical motion in an isentropic coordinate system, given by

$$\frac{d\theta}{dt} = \left(\frac{J}{C_p} \right) e^{xz/H}$$

where J is the diabatic heating rate per unit mass, K is the ratio of the gas constant to specific heat at constant pressure, z is altitude and H is the scale height. Thus positive $d\theta/dt$ indicates ascent.

[18] The horizontal structure of WACCM stratopause temperature and height fields shown in Figures 2a and 2b is similar to observed geographic patterns [i.e., *Thayer et al.*, 2010; F12]. An Aleutian anticyclone is situated over the north Pacific, and the Arctic vortex is displaced to $\sim 60^{\circ}\text{N}$ over Greenland, whereas the climatological vortex is centered at $\sim 80^{\circ}\text{N}$ [e.g., *Waugh and Randel*, 1999; *Mitchell et al.*, 2011; F12]. Stratopause temperature extrema are located along the edge of the polar vortex in the region of strongest winds resulting in large horizontal temperature advection. The stratopause is highest inside the Arctic vortex and lowest inside the Aleutian anticyclone. That the temperature is in quadrature with the height is consistent with ageostrophic vertical motion associated with vertically propagating PW energy [*Wallace*, 1978; *Ambaum and Hoskins*, 2002; *Thayer et al.*, 2010; F12].

[19] The longitude-altitude sections of eddy temperature and eddy $d\theta/dt$ (Figures 2c and 2d) confirm westward tilting wave-1 patterns that align with the vortex and anticyclone throughout the stratosphere and mesosphere. The eddy temperature and $d\theta/dt$ are strongly anti-correlated with a correlation coefficient of -0.90 , which suggests that the temperature anomalies are a result of vertical ageostrophic motions due to vertically propagating PW energy. This results in PW breaking in the upper stratosphere [e.g., *McIntyre and Palmer*, 1983], inertial instability [e.g., *Knox and Harvey*, 2005], wave-wave interactions [e.g., *Smith*, 1983], barotropic instability [e.g., *Simmons et al.*, 1983], and baroclinic instability [e.g., *Thayer et al.*, 2010;

F12], which all contribute to EP flux divergence and likely contribute to the observed ageostrophic flow [e.g., *Andrews et al.*, 1987]. These instabilities result in ageostrophic flow in order to maintain quasi-geostrophic and hydrostatic balance [e.g., *Holton*, 2004], and the respective role of each of these instabilities needs to be further investigated.

3.3. Geographic Patterns in the Climatological Stratopause

[20] Vertically propagating PWs have been shown to be a climatological feature that results in zonal asymmetries in monthly mean stratopause temperature and height [F12]. Having now shown that WACCM reproduces such events, we consider the climatological spatial structure of the stratopause with respect to the mean position of the polar vortices and anticyclones. While the stratopause in WACCM is warmer and higher in the polar winter zonal mean than MLS, we will show that it properly reproduces daily geographic patterns in stratopause temperature and height observed by MLS.

3.3.1. Northern Hemisphere—No Elevated Stratopause Events

[21] Figure 3 shows the Northern Hemisphere (NH) 40 year WACCM and 8 year MLS monthly mean geographic distribution of stratopause temperature and height in December, January, and February (DJF). The thick black (white) contours encompass regions where the vortex (anticyclones) is present for at least 50% and 70% (30% and 70%) of the given month. In general, the WACCM climatology is consistent with MLS and GEOS. Significant features that are similar between the two climatologies during DJF include the following:

- A large Aleutian High is present, and stratopause temperature is lowest along the eastern flank of the anticyclone. Stratopause height is lowest along the western flank of the anticyclone.
- The vortex is displaced toward the Greenwich Meridian consistent with previous work [e.g., *Waugh and Randel*, 1999; *Mitchell et al.*, 2011; F12].

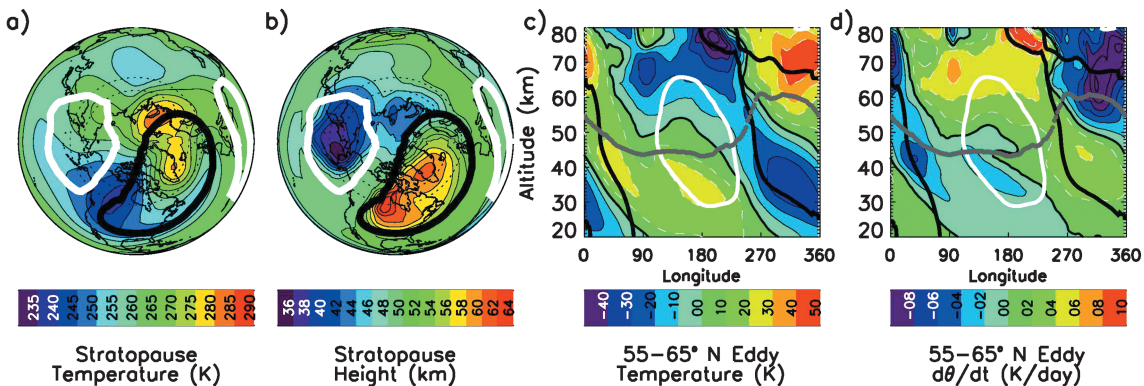


Figure 2. Polar projections of (a) stratopause temperature and (b) stratopause height, and longitude-altitude plots of (c) temperature and (d) $d\theta/dt$ averaged between 55°N and 65°N on 10 December of an arbitrary model year. The Greenwich Meridian is oriented to the right. The polar vortex and anticyclones are indicated by the thick black and white contours, respectively. The gray contour indicates stratopause.

- The stratopause in the Arctic vortex is warmest between 0°E and 90°E .
- From 40°N to the pole, there is a wave-1 structure in stratopause temperature and height.

[22] In both WACCM and MLS, the stratopause height anomalies are 90° out of phase with the temperature anomalies. The separated polar winter stratopause due to GW-driven descent results in a warm and elevated stratopause in the vortex. The warm anomaly is shifted from the vortex core due to upward propagating PWs. The baroclinic PWs result in temperature extrema at the edge of the vortex, consistent with the ageostrophic vertical motion depicted by *Thayer et al.* [2010].

[23] Major differences between WACCM and observations include the following:

- The vortex is 30% spatially smaller in WACCM, with maximum differences of 45% in November (not shown) and minimum differences of 5% in January.
- The stratopause is warmer ($\sim 9\text{--}12\text{K}$) and higher ($\sim 3\text{--}5\text{ km}$) in WACCM, especially inside the Arctic vortex.

[24] The smaller vortex in WACCM likely leads to the warmer temperatures in the vortex, because the global residual circulation (poleward flow in the winter mesosphere and descent in the vortex) is confined to a smaller region, so descent rates would necessarily be larger in order to conserve mass. Thus, the two major differences between the NH stratopause climatology in WACCM and observations can both be attributed to the smaller vortex in

WACCM. It is not fully understood why the polar vortex in WACCM at stratopause altitudes is spatially smaller than observed (R. Garcia, personal communication, 1994).

3.3.2. Southern Hemisphere

[25] Figure 4 shows the 40 year WACCM (left panels) and 8 year MLS (right panels) monthly mean stratopause temperature and height in the Southern Hemisphere (SH) for July, August, and September (JAS). The black and white contours indicate the edge of the Antarctic vortex and anticyclones, respectively, consistent with the contour levels shown in Figure 3. As in the NH analysis, we focus on a comparison of the 40 year WACCM climatology with MLS.

[26] In JAS, the anticyclones in WACCM are located southwest of Australia, consistent with GEOS in August and September and previous work [e.g., *Quintanar and Mechoso*, 1995; *Harvey and Hitchman*, 1996]. The Antarctic vortex is significantly smaller than observed, which allows anticyclones to penetrate to high latitudes earlier in the year. The polar vortex is shifted off the pole toward South America during all 3 months. Low anomalies in stratopause temperatures are inside and to the east of the anticyclone, consistent with observations, suggesting that ageostrophic vertical motion associated with vertically propagating baroclinic PWs is a climatological feature in the SH.

[27] Differences between WACCM and the MLS climatology include the following:

- In the vortex, the WACCM stratopause remains elevated above 58 km through September, whereas MLS shows

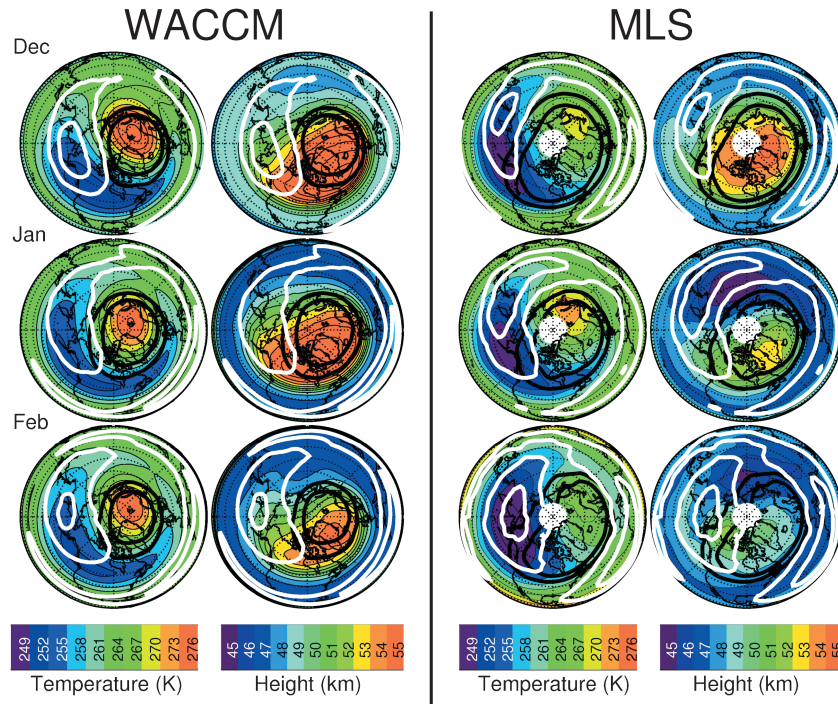


Figure 3. Monthly mean NH polar projections of stratopause temperature and height for December, January, and February from WACCM (left) and MLS (right). The Greenwich Meridian is oriented to the right. Thick black (white) contours encompass regions where the vortex (anticyclones) are present 50% and 70% (30% and 70%) of each month.

the stratopause height descend to ~ 47 km by September. The persistent separated polar winter stratopause in the Antarctic is likely due to too little orographic GW drag in WACCM [e.g., *McLandress et al.*, 2012].

- The vortex at the stratopause is 46% spatially smaller in WACCM than in GEOS, on average, with a maximum difference of 52% in July and a minimum of 22% in March (not shown).
- The stratopause in the vortex is 12–15K warmer in WACCM during July and August. In September, it is 6K warmer than MLS as sunlight returns to the polar region and the dynamically driven stratopause gives way to radiative heating of ozone as the dominant mechanism.

[28] Figure 5 shows polar maps of the WACCM 40 year monthly mean geographic distribution of (a) NH eddy temperature and (b) NH eddy $d\theta/dt$ during January and (c) SH eddy temperature and (d) SH eddy $d\theta/dt$ during August at the stratopause. We only show 1 month for each hemisphere because the patterns in eddy temperature and eddy $d\theta/dt$ are consistent for DJF in the NH and JAS in the SH. The eddy in Figure 5 is determined by subtracting the equivalent latitude zonal mean from each field. The vortex and anticyclones are displayed as in Figures 3 and 4.

[29] The monthly mean stratopause $d\theta/dt$ in both hemispheres (not shown) indicates descent at all latitudes and longitudes poleward of 20° in the winter hemisphere, with largest monthly mean descent rates of ~ 18 K/day occurring in the core of the mid-winter vortex. In the NH, there are negative eddy temperatures inside and to the east of the Aleutian anticyclone extending to the east across Canada and the North Atlantic. Positive anomalies occur in the vortex and are shifted toward the western flank of the Aleutian

anticyclone. These temperature anomalies are coincident with the anomalies in eddy $d\theta/dt$. The $d\theta/dt$ anomalies indicate relatively weak descent in regions of negative temperatures anomalies and enhanced descent in regions of positive stratopause temperature anomalies. The eddy $d\theta/dt$ and eddy temperature in the NH have a correlation of -0.93 . This is consistent with the hypothesis of F12 that vertical motions associated with vertically propagating PWs leads to the observed temperature structure at the stratopause. In the SH during August, negative eddy stratopause temperatures are located at the eastern edge of the Australian anticyclone extending to the east near South America, and positive eddy stratopause temperatures are located between the vortex and the western flank of the Australian anticyclone. As in the NH, eddy temperature anomalies in the SH winter are collocated with anomalies in eddy $d\theta/dt$ and have a correlation of -0.95 during August. These anomaly patterns demonstrate that vertical motions produce asymmetries in stratopause temperatures shown in Figures 3 and 5, consistent with the hypothesis of F12.

3.4. Longitude-Altitude Structure

[30] We next interpret the vertical temperature structure during DJF in the NH and JAS in the SH in the context of the structure of the polar vortices and anticyclones. Figure 6 shows 40 year mean longitude-altitude sections of temperature between 55 and 65°N during DJF (top) and between 45 and 55°S during JAS (bottom) in WACCM (left) and MLS (right). The vortex (anticyclone) contours indicate where they are present 40% and 80% (10% and 50%) of the season. We show these levels to best illustrate the structure of the vortex and anticyclones. The gray line indicates the stratopause. The latitude bands were chosen to best display

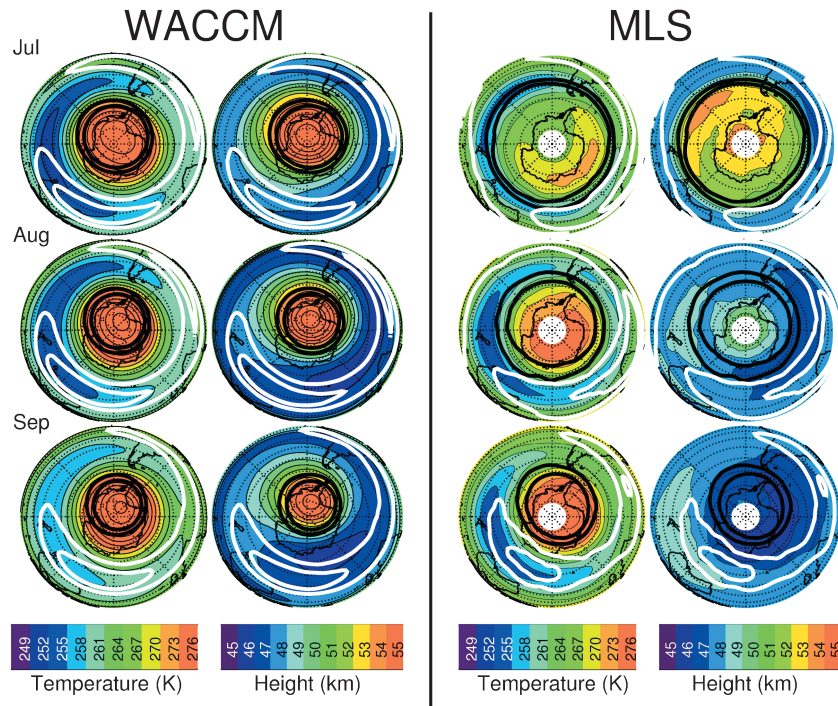


Figure 4. Same as Figure 3 but for the SH in July, August, and September.

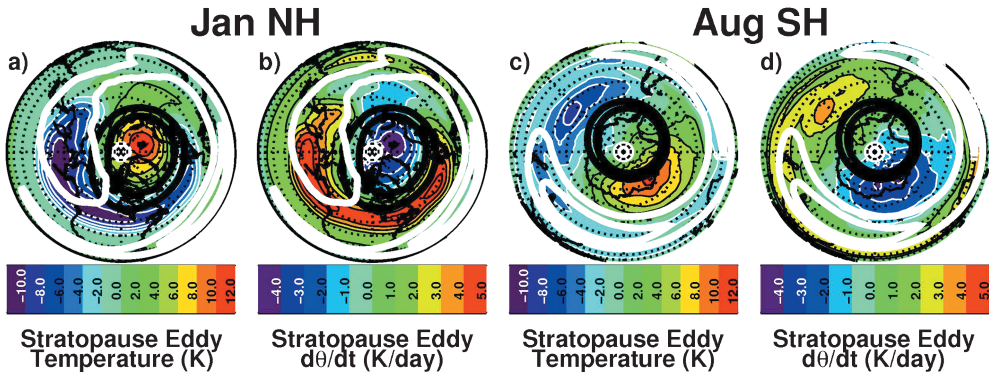


Figure 5. Polar projections of (a) eddy temperature and (b) eddy $d\theta/dt$ (equivalent latitude zonal mean is removed) at the stratopause in the NH during January and (c) eddy temperature and (d) eddy $d\theta/dt$ in the SH during August. Thick black (white) contours encompass regions where the vortices (anticyclones) are present 50% and 70% (30% and 70%) of each month.

the PW activity in each hemisphere. In the SH, the anticyclones are generally confined to lower latitudes than in the NH.

[31] In general, the vertical structure of temperature, the polar vortices, and anticyclones in WACCM are in good agreement with MLS and GEOS. In both hemispheres, the vortex and anticyclones tilt westward with height. The vertical temperature structure shows a distinct association with the location of the

polar vortices and anticyclones. Low temperatures near 240K in the NH and 250K in the SH occur near the eastern edge of the anticyclones and the western edge of the vortex, and warm temperatures near 255K occur in both hemispheres at the western edge of the vortex and eastern edge of the anticyclones. The anticyclones are centered near the Date Line in the NH with the Arctic vortex displaced from the pole toward the Greenwich Meridian. In the SH, the anticyclones are centered at 120°E

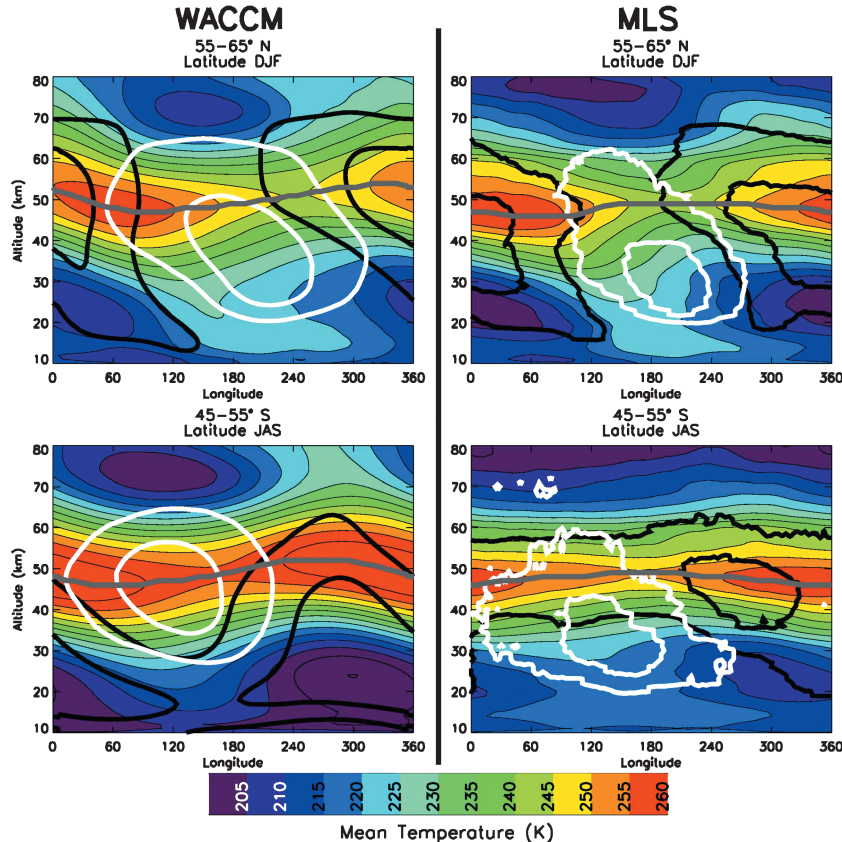


Figure 6. Longitude-altitude plots of WACCM (left) and MLS (right) temperature averaged between 55 and 65°N for DJF (top) and 45–55°S for JAS (bottom). The thick black, white, and gray contours represent the vortex, anticyclones, and stratopause, respectively. The vortex (anticyclone) contours indicate where they are present 40% and 80% (10% and 50%) of the season.

and the Antarctic vortex is displaced into the western hemisphere. In the SH, the vortex and anticyclones are more barotropic compared to that in the NH. This is likely due to fewer disturbances in the SH resulting from less vertically propagating PW energy [e.g., Youn *et al.*, 2006].

[32] Differences between WACCM and the observations include the following:

- In the NH, the wave-1 amplitude in stratopause height in WACCM is over twice that observed by MLS (7 km versus 3 km).
- The Aleutian anticyclone is longitudinally broader at the stratopause; it extends from $\sim 60^{\circ}\text{E}$ to $\sim 270^{\circ}\text{E}$ compared to $\sim 90^{\circ}\text{E}$ to $\sim 220^{\circ}\text{E}$ in observations.
- The Antarctic vortex is smaller at this latitude band compared with observations.

3.5. Temporal Evolution

[33] We now summarize the temporal evolution of stratopause temperature and height inside the polar vortices and anticyclones during the months that the polar vortex is well established at the stratopause. Figure 7 shows the WACCM 40 year daily mean stratopause temperature (left) and height (right) in the vortex (solid black) and anticyclones (solid gray) as a function of time poleward of 40°N in the NH (top) and poleward of 20°S in the SH (bottom). We choose these latitudes in order to reduce influences of low latitude anticyclones, thus focusing the analysis more on the Aleutian and Australian anticyclones,

though we note that mid-latitude anticyclones that are not associated with the climatological anticyclones are included in this analysis. The blue and red regions indicate one standard deviation from the mean stratopause temperature and height in the polar vortices and anticyclones, respectively. The black and gray dashed contours are based on MLS observations in the polar vortices and anticyclones, respectively.

[34] In general, WACCM properly simulates the temporal evolution of stratopause temperature and height in the vortex and anticyclones, particularly in the NH. In the Arctic vortex, the stratopause warms from October to January and cools from January to March (upper left panel). Likewise, both WACCM and MLS show that the stratopause in the Arctic vortex becomes elevated in October to near 58 km and gradually descends throughout the winter (upper right panel). In both hemispheres, the temporal evolution of stratopause temperature and height in NH anticyclones is consistent between WACCM and MLS.

[35] Differences between WACCM and MLS observations include the following:

- In the Antarctic vortex, the stratopause in WACCM is $\sim 20\text{K}$ warmer than observations between April and August.
- In the Antarctic vortex, the stratopause in WACCM is ~ 10 km higher than that in MLS in August and September.
- In the Arctic vortex, the stratopause is 5–15K warmer in WACCM compared to observations.

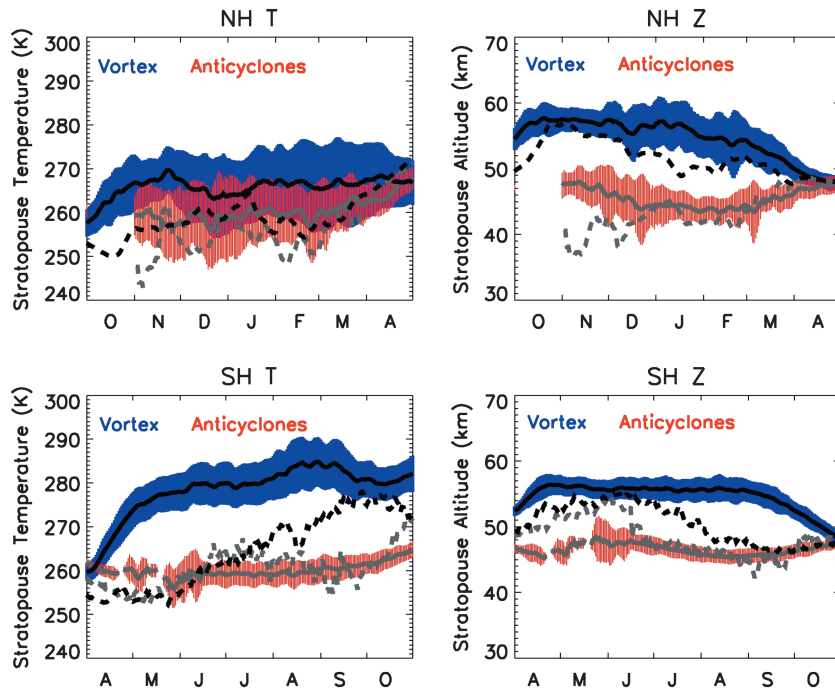


Figure 7. Time series of WACCM stratopause temperature (left) and stratopause height (right) in the NH (top) and SH (bottom). Black and gray lines indicate the 40 year daily mean of the vortex and anticyclones, respectively. Blue and red shading represent one standard deviation from the mean of the daily means in the vortex and anticyclones, respectively. Black and gray dashed lines indicate 8 year average annual cycles based on MLS. NH and SH anticyclones are considered poleward of 40°N and 20°S , respectively.

4. Elevated Stratopause Events

[36] ES events are dynamically different from the stratopause climatology and are considered separately here. ES events in WACCM are always preceded by major SSWs. In the model, major SSWs begin between 7 and 22 days prior to ES onset dates. Major SSWs persist between 0 days and 26 days after ES onset. In the observations, ES events occur 15 days and 11 days following the onset of the major SSWs in 2006 and 2009, respectively. The 2012 ES event occurred following 31 days in which minor SSW conditions were met. A common theme in both the model and observations is that ES events occur during prolonged disturbed periods (11 to 47 days in WACCM and 27 to 32 days in the observations). Using the method described in section 2, we identified 15 ES events in the 40 year WACCM simulation, or an average of 0.375 ES events per winter. We identify three ES events observed by MLS during the eight NH winters (0.375 ES events per winter) between November 2004 and March 2012 (ES onset dates are on 30 January 2006, 5 February 2009, and 30 January 2012). This frequency of occurrence is consistent with the rate given by *de la Torre et al.* [2012] and *Chandran et al.* [2013], who found that ES events occur 2 to 4 times per decade in WACCM. On average, the stratopause remains elevated for ~23 days following an event onset, with a range of 6 to 75. We also apply this method to eight winters of MLS data between November 2004 and April 2012, and find three ES events.

[37] Figure 8 shows the average number of days per month that the stratopause is considered elevated in WACCM (red) and MLS (black) between December 2004 and May 2012. While the seasonal frequency of ES events is consistent between WACCM and MLS, this shows that ES events occur most often in WACCM in December. Because SSWs occur between 1 and 3 weeks prior to the onset of the ES events, this result is consistent with *de la Torre et al.* [2012; Figure 2], who found that the occurrence of SSWs in WACCM peaks in November. They also found that the only statistically significant difference between WACCM and NCEP/NCAR reanalysis data is associated with vortex splitting events. This suggests that the PW-2 amplitudes become unrealistically large in WACCM in November and December, leading to vortex splitting event SSWs and ES events 1 month before they occur in observations. MLS shows a peak occurrence of ES days in February and no ES days in November or December.

[38] Figure 9 shows the evolution of composite mean stratopause temperature and height for the 15 ES events in WACCM (left) and the ES event in 2012 observed by MLS (right). The top panels show the 30 days prior to the ES onset (1–30 January 2012 for the MLS case), and the bottom panels include the 30 days following the ES onset (31 January–29 February 2012 for MLS). The white dots with smaller red dots superimposed in the stratopause height plots indicate the maximum stratopause height poleward of 20°N for the 30 day mean before and after each event. In the temperature plots, these symbols indicate the poleward-most local temperature maximum for the 30 day mean of each event. This prevents flagging low latitude temperature maxima that are not associated with the ES.

[39] Prior to the ES events (top row), the structure of the stratopause temperature and height in WACCM is similar

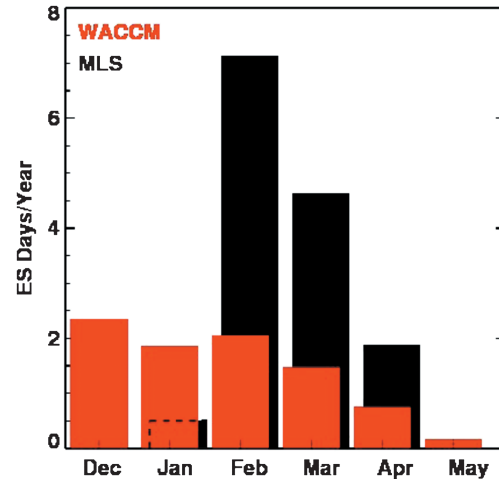


Figure 8. Histogram of the average number of ES days per month from December to May in WACCM (red) and MLS (black).

to what is shown in December–February in Figure 3. The stratopause in MLS prior to the 2012 ES is similar to what is shown in the January climatology in F12 (see their Figure 3). In both MLS and WACCM, the longitudinal offset between temperature extremes and the circulation suggests that ageostrophic vertical motions due to vertically propagating PWs dominate during this period. The Aleutian anticyclone is well established at high latitudes over the Date Line, and the Arctic vortex is displaced from the pole toward the Greenwich Meridian.

[40] In the 30 days following the ES events (bottom row), both MLS and WACCM show that the ES is neither pole centered nor vortex centered but rather is highest over the Canadian Arctic. The highest stratopause temperatures occur to the east of Greenland in the vortex and are displaced 90° to the east over the Norwegian Sea. The offset stratopause temperatures are consistent with *Manney et al.* [2005], who used GEOS-4 to show that the temperature maximum was similarly displaced from the pole during February at 1700K (~1 hPa) following the 2004 major SSW. The large vortex that occurs during this period is also consistent with previous studies of ES events [e.g., *Manney et al.*, 2008]. The reformation of the ES at mesospheric altitudes is attributed to non-orographic GW drag in the mesosphere [*Siskind et al.*, 2007; 2010; *Limpasuvan et al.*, 2011; *Ren et al.*, 2011]. Thus, zonal asymmetries in non-orographic GW forcing is likely responsible for the asymmetries in ES stratopause height modeled by WACCM and observed by MLS. Since ES events are often neither pole centered nor zonally symmetric, caution should be used when diagnosing them using polar cap averages or zonal mean.

[41] Figure 10 shows the composite mean vertical structure of temperature for the 15 ES events in WACCM (left) and the ES event in 2012 observed by MLS (right) between 70 and 80°N. The top panels show the 30 days prior to ES onset dates (1–30 January 2012 for the MLS case), and the bottom panels include the 30 days following ES onset dates (31 January–29 February 2012 for MLS). Prior to the onset of ES events, both WACCM and MLS show a vertical structure that is consistent with what is shown for the climatological mean in Figure 6. The

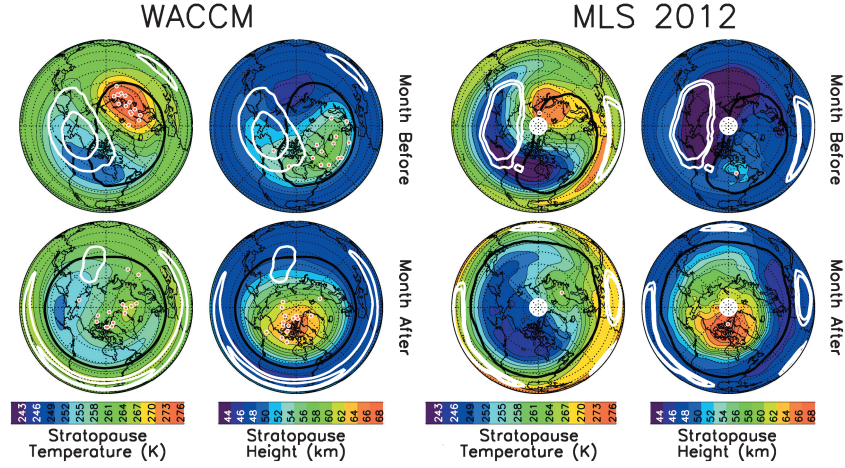


Figure 9. Polar projections of the WACCM ES composite (left) and the ES event in 2012 observed by MLS (right). Red dots outlined in white indicate the maximum stratopause height poleward of 20°N for the 30 day mean of each event. In the temperature plots, the symbols indicate the poleward most local temperature maximum for the 30 day mean of each event. Thick black (white) contours represent the vortex (anticyclone) edges. Thick black (white) contours encompass regions where the vortex (anticyclones) are present 50% and 70% (30% and 70%) of the time.

wave-1 pattern in temperature and the westward tilt of the vortex and anticyclones is consistent with upward propagating PW energy. The stratopause is 5–10K warmer

compared to the climatology, suggesting enhanced PW energy which leads to stronger vertical motion and adiabatic warming.

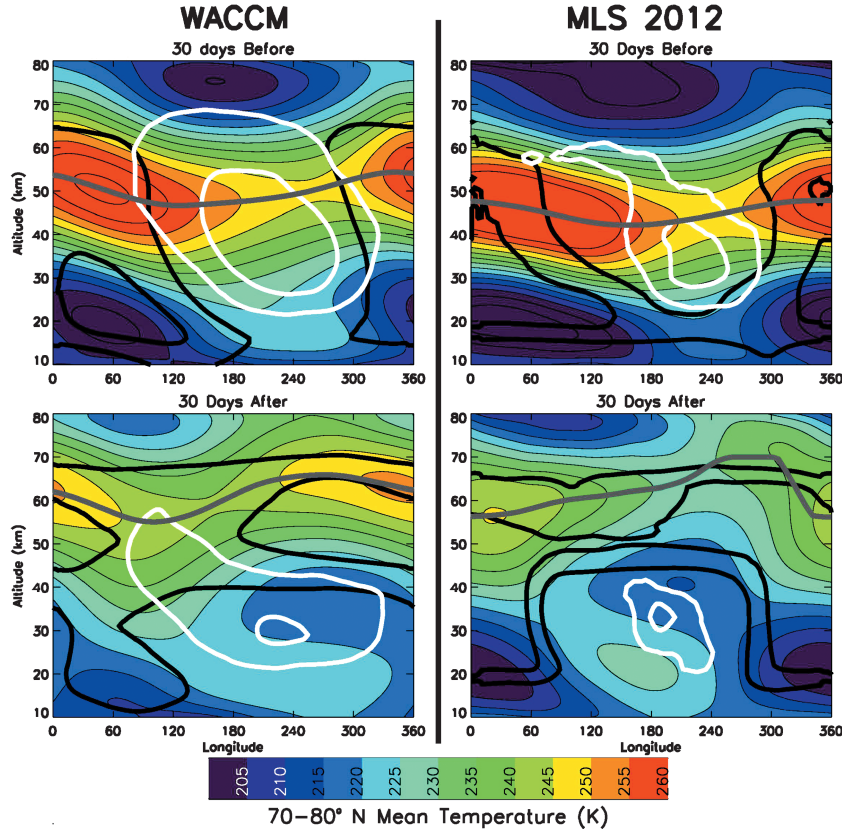


Figure 10. Longitude-altitude plots of ES composite WACCM (left) and 2012 MLS (right) temperature averaged between 70 and 80°N for 30 days before ES onset (top) and 30 days after ES onset (bottom). The thick black, white, and gray contours represent the vortex, anticyclones, and stratopause, respectively. The vortex (anticyclone) contours indicate where they are present 40% and 80% (10% and 50%) of the time.

[42] In the month following ES onset dates (bottom panels), PWs continue to tilt westward with altitude between the tropopause to the upper stratosphere suggesting that PW energy continues to propagate upward. However, in the month following ES onset dates, the stratopause is \sim 15K cooler than that in the month before ES onset dates. A colder stratopause is consistent with the theory that ES events occur post-disturbance, thus resulting in weaker ageostrophic vertical motions. At stratopause altitudes, the vortex is present at all longitudes in the $65\text{--}75^\circ\text{N}$ latitude band, while below 40 km, the vortex is confined to a 120° longitude band between 0°E and 120°E in WACCM and 300°E and 60°E in MLS. The location of the lower stratospheric vortex is likely responsible for the offset of the ES from the pole shown in Figure 9. Vertically propagating GWs with easterly phase speed propagate vertically through the stratospheric vortex and break in the mesosphere, leading to poleward and downward flow [e.g., Lindzen, 1981]. Because the vortex is longitudinally confined, these vertically propagating GWs are also confined and result in the observed ES structure. The hypothesis that 3-D gravity wave drag is responsible for longitudinal variability near the stratopause is mentioned in Harvey and Hitchman [1996].

5. Conclusions

[43] In this work, we show a 40 year climatology of stratopause temperature and height in WACCM and interpret geographic structures with respect to the location of the polar vortices and anticyclones. We compare the 40 year WACCM climatology to an 8 year climatology based on MLS observations. We show the seasonal and geographic distribution of stratopause temperature and height and demonstrate that ageostrophic vertical motion associated with baroclinic PWs results in the climatological structure of the stratopause. In general, the WACCM results shown here are in agreement with MLS.

[44] We show a case study of stratopause temperature, height, and $d\theta/dt$, in which a westward tilting PW drives ageostrophic motion including descent and warming east of the vortex and ascent and cooling east of the anticyclone. Specifically, anticyclones move from low latitudes eastward and poleward, displacing the vortex off the pole and creating baroclinic conditions. Ageostrophic vertical motion arises to maintain quasi-geostrophic and hydrostatic balance in the presence of westward tilting PWs, and this leads to the observed temperature anomalies.

[45] In the NH, WACCM shows the mean climatological vortex to be displaced over Northeast Greenland in December, January, and February. Stratopause temperature maxima are not vortex centered but shifted into the Eastern Hemisphere. The stratopause is coldest from the center of the Aleutian anticyclone (over the North Pacific) extending to the east over Canada. In the SH, the stratopause is highest and warmest inside the Antarctic vortex. The stratopause is coldest from the center of the Australian anticyclone over the South Pacific and to South America. These structures are consistent with MLS observations of stratopause geography.

[46] Due to ES events being dynamically distinct from undisturbed periods, they are considered separately in this

analysis. An ES composite of stratopause temperature and height is constructed using 15 ES events identified in WACCM and compared to the 2012 ES event observed by MLS. WACCM simulates ES events in December that are not observed by MLS. During the month prior to ES events, the temperature and height structure of the polar winter stratopause demonstrates a clear signature of ageostrophic vertical motion arising from baroclinic PWs in both model results and observations. In the month following ES events, the maximum height of the stratopause is not pole centered but is displaced over the Canadian Arctic. The stratopause is warmest 90° east of the height maximum over the Norwegian Sea. This is the first work to show zonal asymmetries in stratopause temperature and height during ES events. The WACCM ES composite, combined with the 2012 ES event observed by MLS, demonstrates that ES events are not always pole centered or zonally symmetric and care should be taken when using polar cap averages or zonal mean quantities.

[47] Results from WACCM are generally consistent with observations and clearly demonstrate the observed geographic anomalies in stratopause temperature and height as well as the vertical motions that lead to these anomalies. While the WACCM climatology effectively reproduces the main features of the observed stratopause climatology, notable differences include

- The vortex at the stratopause is geographically 30% smaller in the NH and 45% smaller in the SH in WACCM.
- The Antarctic vortex in WACCM persists 1 month longer at the stratopause than in GEOS.
- The SH stratopause in the vortex is, on average, 13K warmer and 6 km higher in WACCM than in observations.

[48] **Acknowledgments.** We thank Ethan D. Peck for providing us with the WACCM simulation. We thank Rolando Garcia for help interpreting the WACCM results. This work was funded under NASA grant NNX08AK45G, NSF CEDAR grant AGS 0940124, and NSF ARC grant 1107498.

References

- Andrews, D. G., J. R. Holton, and C. B. Leovy (1987), Middle Atmosphere Dynamics, Academic Press, Orlando, Florida, 489 pp.
 Ammann, Maarten H. P., and Brian J. Hoskins (2002), The NAO Troposphere-Stratosphere Connection, *J. Climate*, **100**, 505–530, doi:10.1175/1520-0442(2002)015<1969:TNTSC>2.0.CO;2.
 Barnett, J. J. (1974), The mean meridional temperature behaviour of the stratosphere from November 1970 to November 1971 derived from measurements by the Selective Chopper Radiometer on Nimbus IV, *Quart. J. Roy. Meteorol. Soc.*, **100**, 505–530, doi: 10.1002/qj.49710042602.
 Becker, E. (2012), Dynamical control of the middle atmosphere, *Space Sci. Rev.*, doi:10.1007/s11214-011-9841-5.
 Beres, J. H., R. R. Garcia, B. A. Boville, and F. Sassi (2005), Implementation of a GW source spectrum parameterization dependent on the properties of convection in the Whole Atmosphere Community Climate Model (WACCM), *J. Geophys. Res.*, **110**, D10108, doi:10.1029/2004JD005504.
 Braesicke, P., and U. Langematz (2000), On the occurrence and evolution of extremely high temperatures at the polar winter stratopause—A GCM study, *Geophys. Res. Lett.*, **27**(10), 1467–1470, doi:10.1029/2000GL011431.
 Chandran, A., R. L. Collins, R. R. Garcia, and D. R. Marsh (2011), A case study of an elevated stratopause generated in the Whole Atmosphere Community Climate Model, *Geophys. Res. Lett.*, **38**, L08804, doi:10.1029/2010GL046566.
 Chandran, A., et al. (2013), A climatology of elevated stratopause events in the Whole Community Climate Model, *J. Geophys. Res.* doi:10.1002/jgrd.50123.

- Charlton, A. J., et al. (2007), A new look at stratospheric sudden warmings. Part II: Evaluation of numerical model simulations, *J. Climate*, 20, 470–488, doi:10.1175/JCLI3994.1.
- Charlton, A. J., and L. M. Polvani (2007), A new look at stratospheric sudden warmings. Part I: Climatology and modeling benchmarks. *J. Climate*, 20, 449–469.
- Charney, J. G., and P. G. Drazin (1961), Propagation of planetary-scale disturbances from the lower into the upper atmosphere, *J. Geophys. Res.*, 66, 83–109.
- Day, K. A., R. E. Hibbins, and N. J. Mitchell (2011), Aura MLS observations of the westward-propagating $s=1$, 16-day planetary wave in the stratosphere, mesosphere and lower thermosphere, *Atmos. Chem. Phys.*, 11, 4149–4161.
- de la Torre, L., R. R. Garcia, D. Barriopedro, and A. Chandran (2012), Climatology and characteristics of stratospheric sudden warmings in the Whole Atmosphere Community Climate Model, *J. Geophys. Res.*, 117, D04110, doi:10.1029/2011JD016840.
- Dritschel, D. G. (1993), A fast contour dynamics method for many vortex calculations in two-dimensional flows, *Phys. Fluids*, 5A, 173–186.
- Fleming, E. L., S. Chandra, J. J. Barnett, and M. Corney (1990), Zonal mean temperature, pressure, zonal wind and geopotential height as functions of latitude, *Adv. Space Res.*, 10, 1211–1259.
- France, J. A., V. L. Harvey, C. E. Randall, M. H. Hitchman, and M. J. Schwartz (2012), A climatology of stratopause temperature and height in the polar vortex and anticyclones, *J. Geophys. Res.*, 117, D06116, doi:10.1029/2011JD016893.
- Garcia, R. R., and B. A. Boville (1994), Downward control of the mean meridional circulation and temperature distribution of the polar winter stratosphere, *J. Atmos. Sci.*, 51, 2238–2245, doi:10.1175/1520-0469(1994)051<2238:COTMMC>2.0.CO;2.
- Garcia, R. R., D. R. Marsh, D. E. Kinnison, B. A. Boville, and F. Sassi (2007), Simulation of secular trends in the middle atmosphere, 1950–2003, *J. Geophys. Res.*, 112(D9), D09301, doi:10.1029/2006JD007485.
- Hannachi, A., D. Mitchell, L. Gray, and A. Charlton-Perez (2011), On the use of geometric moments to examine the continuum of sudden stratospheric warmings, *J. Atmos. Sci.*, 68, 657–674.
- Harvey, V. L., and M. H. Hitchman (1996), A climatology of the Aleutian High, *J. Atmos. Sci.*, 53, 2088–2102.
- Harvey, V. L., et al. (2002), A climatology of stratospheric polar vortices and anticyclones, *J. Geophys. Res.*, 107(D20), 4442, doi:10.1029/2001JD001471.
- Harvey, V. L., C. E. Randall, and M. H. Hitchman (2009), Breakdown of potential vorticity-based equivalent latitude as a vortex-centered coordinate in the polar winter mesosphere, *J. Geophys. Res.*, 114, D22, doi:10.1029/2009JD012681.
- Hitchman, M. H., and C. B. Leovy (1986), Evolution of the zonal mean state in the equatorial middle atmosphere during October 1978–May 1979, *J. Atmos. Sci.*, 43, 3159–3176.
- Hitchman, M. H., et al. (1989), The separated polar winter stratopause: A gravity wave driven climatological feature, *J. Atmos. Sci.*, 46, 410–422.
- Holton, J. R. (2004), An Introduction to Dynamic Meteorology, 4th Edition, Elsevier Academic Press, New York, New York.
- Hood, L. L. (1986), Coupled stratospheric ozone and temperature response to short-term changes in solar ultraviolet flux: An analysis of Nimbus 7 SBUV and SAMS data, *J. Geophys. Res.*, 91, 5264–5276.
- Kinnison, D. E., et al. (2007), Sensitivity of chemical tracers to meteorological parameters in the MOZART-3 chemical transport model, *J. Geophys. Res.*, 112, D20302, doi:10.1029/2006JD007879.
- Knox, J., and V. L. Harvey (2005), Global climatology of inertial instability and Rossby wave breaking in the stratosphere. *J. Geophys. Res.*, 110, doi:10.1029/2004JD005068.
- Kvissel, O., et al. (2011), Mesospheric intrusion and anomalous chemistry during and after a major stratospheric sudden warming, *J. Atmos. Sol.-Terr. Phys.*, 78–79, 116–124, doi:10.1016/j.jastp.2011.08.015.
- Labitzke, K. (1974), The temperature in the upper stratosphere: Differences between hemispheres, *J. Geophys. Res.*, 79, 2171–2175.
- Limpasuvan, V., et al. (2011), The roles of planetary and gravity waves during a major stratospheric sudden warming as characterized in WACCM, *J. Atmos. Sol.-Terr. Phys.*, doi:10.1016/j.jastp.2011.03.004.
- Lin, S.-J. (2004), A “vertically-Lagrangian” finite-volume dynamical core for global atmospheric models, *Mon. Wea. Rev.*, 132, 2293–2307.
- Lindzen, R. S. (1981), Turbulence and stress owing to gravity wave and tidal breakdown, *J. Geophys. Res.*, 86, 9707–9714.
- Livesey, N. J., et al. (2011), Earth Observing System (EOS) Microwave Limb Sounder (MLS) Version 3.3 Level 2 data quality and description document, Rep. JPL D-33509, Jet Propul. Lab., Pasadena, Calif.
- Manney, G. L., et al. (2005), The remarkable 2003–2004 winter and other recent warm winters in the Arctic stratosphere since the late 1990s, *J. Geophys. Res.*, 110, D04107, doi:10.1029/2004JD005367.
- Manney, G. L., et al. (2008), The evolution of the stratopause during the 2006 major warming: Satellite data and assimilated meteorological analyses, *J. Geophys. Res.*, 113, D11115, doi:10.1029/2007JD009097.
- Manney, G. L., et al. (2009), Aura Microwave Limb Sounder observations of dynamics and transport during the record-breaking 2009 Arctic stratospheric major warming, *Geophys. Res. Lett.*, 36, L12815, doi:10.1029/2009GL038586.
- Marsh, D. (2011), Chemical-dynamical coupling in the mesosphere and lower thermosphere, *Aeronomy of the Earth’s Atmosphere and Ionosphere*, Ali Ali Abdu, M., Pancheva, D., Eds. Springer, New York, NY.
- Matthewman, N., J. Esler, A. Charlton-Perez, and L. Polvani (2009), A new look at stratospheric sudden warmings. Part III: Polar vortex evolution and vertical structure, *J. Climate*, 22, 1566–1585.
- McDonald, A. J., Hibbins, R. E., and J. M. Jarvis (2011), Properties of the quasi-16 day wave derived from EOS MLS observations, *J. Geophys. Res.*, 116(479), D06112, doi:10.1029/2010JD014719.
- McFarlane, N. A. (1987), The effect of orographically excited gravity wave drag on the general circulation of the lower stratosphere and troposphere, *J. Atmos. Sci.*, 44, 1775–1800.
- McIntyre, M. E., and T. N. Palmer (1983), Breaking planetary waves in the stratosphere, *Nature*, 305, 593–600.
- McLandress, C., T. G. Shepherd, S. Polavarapu, and S. R. Beagley (2012), Is missing orographic gravity wave drag near 60°S the cause of the stratospheric zonal wind biases in chemistry–climate models?, *J. Atmos. Sci.*, 69, 802–818.
- McLandress, C., and J. F. Scinocca (2005), The GCM response to current parameterizations of nonorographic gravity wave drag, *J. Atmos. Sci.*, 62, 2394–2413.
- Melander, M. V., N. J. Zabusky, and A. S. Styczek (1986), A moment model for vortex interactions of the two-dimensional Euler equations. I: Computational validation of a Hamiltonian elliptical representation, *J. Fluid Mech.*, 167, 95–115.
- Mitchell, D. M., L. G. Gray, and A. J. Charlton-Perez (2011), Characterizing the variability and extremes of the stratospheric polar vortices using 2D moment analysis, *J. Atmos. Sci.*, 68, 1194–1213.
- Nash, E. R., P. A. Newman, J. E. Rosenfield, and M. R. Schoeberl (1996), An objective determination of the polar vortex using Ertel’s potential vorticity, *J. Geophys. Res.*, 101(D5), 9471–9478, doi:10.1029/96JD00066.
- Quintanar, A. I., and C. R. Mechoso (1995), Quasi-stationary waves in the Southern Hemisphere. Part I: Observational data, *J. Clim.*, 8, 2659–2672.
- Ren, S., S. Polavarapu, S. R. Beagley, Y. Nezlin, and Y. J. Rochon (2011), The impact of gravity wave drag on mesospheric analyses of the 2006 stratospheric major warming, *J. Geophys. Res.*, 116, D19116, doi:10.1029/2011JD015943.
- Rienecker, M. M., et al. (2007), The GEOS Data Assimilation System—Documentation of Versions 5.0.1 and 5.1.0, Rep. NASA/TM-2007-104606, 67(1), 92 pp., NASA Goddard Space Flight Cent., Greenbelt, Md.
- Richter, J. H., F. Sassi, and R. R. Garcia (2010), Toward a physically based gravity wave source parameterization in a general circulation model, *J. Atmos. Sci.*, 67(1), 136–156, doi:10.1175/2009JAS3112.1.
- Schwartz, M. J., et al. (2008), Validation of the Aura Microwave Limb Sounder temperature and geopotential height measurements, *J. Geophys. Res.*, 113, D15S11, doi:10.1029/2007JD008783.
- Simmons, A. J., J. M. Wallace, and G. W. Branstator (1983), Barotropic wave propagation and instability, and atmospheric teleconnection patterns, *J. Atmos. Sci.*, 40, 1363–1392.
- Siskind, D. E., et al. (2007), On recent interannual variability of the Arctic winter mesosphere: Implications for tracer descent, *Geophys. Res. Lett.*, 34, L09806, doi:10.1029/2007GL029293.
- Siskind, D. E., S. D. Eckermann, J. P. McCormack, L. Coy, K. W. Hoppel, and N. L. Baker (2010), Case studies of the mesospheric response to recent minor, major, and extended stratospheric warmings, *J. Geophys. Res.*, 115, D00N03, doi:10.1029/2010JD014114.
- Smith, A. K. (1983), Observation of wave-wave interactions in the stratosphere, *J. Atmos. Sci.*, 40, 2484–2496.
- Sun, L. (2010), Downward influence of stratospheric final warming events in an idealized model, Ph.D. Thesis, University of Illinois at Urbana–Champaign, 133 pp.
- Thayer, J. P., K. Greer, and V. L. Harvey (2010), Front-like behavior in the Arctic wintertime upper stratosphere and lower mesosphere, *J. Geophys. Res.*, 115, D00N04, doi:10.1029/2010JD014278.
- Volodin, E. M., and G. Schmitz (2001), A troposphere-stratosphere-mesosphere general circulation model with parametrization of gravity waves: Climatology and sensitivity studies, *Tellus, Ser. A*, 53, 300–316.
- Wallace, J. M. (1978), Trajectory slopes, countergradient heat fluxes and mixing by lower stratospheric waves, *J. Atmos. Sci.*, 35, 554–558.

- Waters, J. W., et al. (2006), The Earth Observing System Microwave Limb Sounder (EOS MLS) on the Aura satellite, *IEEE Trans. Geosci. Remote Sens.*, *44*, 1075–1092, doi:10.1109/TGRS.2006.873771.
- Waugh, D. (1997), Elliptical diagnostics of stratospheric polar vortices, *Quart. J. Roy. Meteor. Soc.*, *123*, 1725–1748.
- Waugh, D., and W. Randel (1999), Climatology of Arctic and Antarctic polar vortices using elliptical diagnostics, *J. Atmos. Sci.*, *56*, 1594–1613.
- Youn, D., W. Choi, H. Lee, and D. J. Wuebbles (2006), Interhemispheric differences in changes of long-lived tracers in the middle stratosphere over the last decade, *Geophys. Res. Lett.*, *33*, L03807, doi:10.1029/2005GL024274.